Comparison of Supersonic Combustion Tests with Shock Tunnels, Flight and CFD

J. Steelant*, A. Mack†
ESTEC, ESA, 2200 AG Noordwijk, The Netherlands

K. Hannemann‡ and A.D. Gardner§
DLR German Aerospace Center, 37073 Göttingen, Germany

In 2002, the HyShot supersonic flight experiment was successfully launched and allowed to access experimental flight data for supersonic combustion. Ground based testing performed in the High Enthalpy Shock Tunnel (HEG) of the German Aerospace Center (DLR) allowed to reproduce the Mach 7.8 flight conditions. The present numerical work focuses on the computation of the experiments in HEG considering flows with and without combustion and fuel injection. Further, variations of the equivalence ratio and the resulting influence on the flow topology are studied.

I. Introduction

Flight testing, CFD, and ground testing are the basis for future scramjet engine development. Ground testing concentrates on reproducing the key features of engine operation, without the cost and engineering challenges associated with flight testing. Experiments have shown that free piston driven shock tunnels are well suited for scramjet testing[1], however comparison with flight tests is necessary.

The HEG free piston driven shock tunnel at DLR Göttingen, has been modified to simulate the free stream conditions encountered during the HyShot flight test, and to permit hydrogen fuelled scramjet testing[2].

The second flight of the HyShot flight test program[3] on 30 July 2002, used a simple, internally ducted supersonic combustion demonstrator model to provide data to crosscheck CFD and ground testing investigations with flight experiments. A Terrier-Orion two-stage sounding rocket boosted the experiment to an apogee of 315km. The payload subsequently gathered speed during re-entry, allowing testing at Mach 7.8 from 37km to 23km altitude.

The flight model inlet was a 18° wedge, and the combustion chamber was rectangular (75mm by 9.8mm) in cross section. The boundary layers and shocks generated on the inlet wedge and sidewalls were bled from the ducted flow to achieve a homogenous inflow to the combustion chamber. Cold, gaseous hydrogen was ejected from four portholes at the front of the combustion chamber. Two combustion chambers, instrumented with 14 pressure transducers per chamber, were used to gather fuel-on and fuel-off data for each point in the flight. Only one chamber was equipped with fuel injectors.

The 1:1 scale ground test model (Fig. 1) also includes two combustors instrumented with 15 pressure transducers and 13 thermocouple heat transfer gauges per chamber. In contrast to the flight configuration, the upper and lower part of the wind tunnel model can individually be put at an angle of attack. This model is designed so that both chambers can be used simultaneously in the HEG, and a single engine module can be tested in the smaller T4 free piston driven shock tunnel of The University of Queensland. A detailed description of the model is given by Gardner and Hannemann[4]; the geometry including the four porthole injectors is shown in Figure 2.

In the present paper, comparisons will be made for the flow conditions corresponding to 27.1 km altitude during the flight test.

II. Previous Results

The data resulting from the HyShot II flight and the HEG experiments are discussed by Gardner and Hannemann[4] and Gardner et al[5]. The comparison of pressure distributions measured in HEG in the fuel-off and fuel-on

* Research Engineer, ESA-ESTEC, Division of Propulsion and Aerothermodynamics
† Internal Research Fellow, ESA-ESTEC, Division of Propulsion and Aerothermodynamics
‡ Head, Spacecraft Section, DLR, Institute of Aerodynamics and Flow Technology
§ Research Engineer, High Speed Configuration Section, DLR, Institute of Aerodynamics and Flow Technology

combustors using different angles of attack (3.6 and 6 degrees) and equivalence ratios (Φ=0, 0.32, 0.35) with the data obtained in flight is plotted together with data resulting from inviscid and viscous (using the Spalart-Allmaras turbulence model) numerical fuel off computations in Figure 3. A significant difference in pressure level exists between HEG and flight related to the fuel-off combustor. The pressure level measured in HEG could be confirmed by the application of analytical methods and CFD. The difference between the fuel-off chamber pressure levels at 27.1 km might be caused by an increasing geometry change of the cowl and combustion chamber leading edges due to ablation in flight. However, the justification of this explanation requires more detailed investigations. Comparing the pressure distribution obtained in HEG at the same angle of attack and equivalence ratio, as determined for the corresponding flight condition, shows that the pressure level obtained in flight can only be reached at the downstream end of the combustor. In the first part of the combustor, the pressure rise is more gradual in HEG compared to the flight data. However, the additional pressure distributions indicate that the pressure plateau measured in flight can be reproduced in HEG by increasing the equivalence ratio by 10 % or the angle of attack by 66 %. The comparison of the normalized pressure distributions in the fuel-off and the fuel-on combustors obtained in HEG using air and nitrogen as a test gas (not shown) and their evaluation by applying analytical and engineering correlations and the performance of equilibrium combustion calculations strongly indicates that the flow in the fuel-on duct remains supersonic with combustion.

In order to further investigate the differences found in the comparison between flight and HEG data and open issues concerning the flow topology in the HyShot combustors, additional ground testing including flow visualization and detailed CFD analyses is required. The present numerical investigations represent the first step of computing the three dimensional flow in the fuel-on and fuel-off HyShot combustors using the DLR TAU code. For these investigations the duct flow has been treated as turbulent flow, however no interaction of the turbulence and the combustion process was taken into account. The complexity of the modeling of the supersonic combustion will be increased step by step in future investigations in order to be able to judge the influence of each additional feature taken into account in the model.

III. Numerical Modelling

The CFD solutions are achieved with the unstructured DLR TAU-Code that has been validated in the past for different configurations at super- and hypersonic flow conditions[6], including extensive studies of wall jets[7, 8] and combustion[9]. The time-accurate three-dimensional Navier-Stokes equations are solved for steady or unsteady flows by an explicit three stage Runge-Kutta scheme or an implicit LUSGS scheme. Different 2nd order upwind solvers such as Van-Leer, AUSM and AUSMDV and gas modelling formulations for perfect gas, thermo-chemical equilibrium and nonequilibrium are available. State of the art acceleration techniques such as local time stepping, residual smoothing and multigrid are implemented. The present calculations have been performed using the Schexnayder finite rate reaction data set[10] with 7 species and 8 reactions. All computations are performed assuming fully turbulent wall boundaries using the Spallart-Allmaras turbulence model with Edwards modification. The wall temperature was fixed at 300K. Due to the fact that the fuel is injected by four discrete holes, the injection, mixing and combustion process has to be modelled three-dimensionally (Figure 2). In spanwise direction, the computational domain (shown in Figure 2) extends from the middle of one fuel injector to the middle between two fuel injectors. At the spanwise boundaries, symmetry conditions are used. In streamwise direction, the whole configuration (inlet, combustor and nozzle) is included in the integration domain. The calculations are achieved on a structured grid and no adaptation is used. The grid contains approximately 10^6 nodes.

IV. Results

The present numerical investigations focus on the HEG operating condition XI which simulates the HyShot flight at an altitude of 27 km and the corresponding HEG runs 663, 664, 667 and 672 (Gardner and Hannemann[4)]. In front of the injection, the shock system originating from the lower combustion chamber wall leading edge is almost 2D. However, the fuel injection displaces the mainly parallel duct flow of the combustion chamber significantly. In front of the injector, a detached bow shock with a corresponding separation on the wall is present. Further downstream, the bow shocks generated upstream of the injectors are reflected at the upper and lower combustion chamber walls and a highly 3D-oblique shock system occurs inside the combustion chamber. Depending on the equivalence ratio and therefore the hydrogen injection pressure, the penetration of the hydrogen into the duct varies and changes the shock pattern. The resulting difference in shock boundary layer interactions, changes the flow topology significantly. In order to predict the combustion process adequately it is essential to capture the influence of these phenomena correctly.

In a first step, run 667 of HEG (Φ=0.25) was numerically computed with the combustion processes switched off. The flow field topology is shown by pressure isolines, streamlines and temperature (Figure 4) and Mach number

(Figure 5) in the injection plane and the spanwise symmetry plane. The shock generated at the combustor leading edge and its reflections can clearly be seen. The bow shock of the hydrogen injection impinges on the upper wall, interacts with the boundary layer but does not lead to separation. The separation in front of the injector is mainly restricted to the injection area. Further down the duct, the shock reflections vanish when interacting with the injected hydrogen. The penetration depth for this case is low. Compared with the boundary layer thickness, the penetration depth at the lower wall is twice as high. Compared to the dimensions of the duct, the penetration extends to approximately 25% of the duct height. At the downstream end of the duct, a mixture temperature of 1100 A K is reached.

Considering the effects of combustion for run 667, Mach number and temperature plots indicate no major impact on the flow topology (Figures 6 and 7). The combustion process starts at x=0.08 and the temperature increases in the injection plane to 2300 K at the duct exit. At this point a combustion efficiency of 76% is reached and combustion is also observed downstream in the nozzle. It is observed that combustion takes place at the mixing interface between the duct flow and the injected hydrogen and therefore it is concluded that the combustion process is mixing dominated. Due to the low equivalence ratio of 0.25 only a portion of the oxygen is burned. Based on the results shown in Figure 7, it can be concluded that the combustion takes place in supersonic flow; the Mach number stays well supersonic away from the walls. No recirculation zones or subsonic areas occur.

The temperature distribution for run 663 (Φ=0.35) in Figure 8 shows slightly higher penetration of the fuel into the duct. Compared with run 667, combustion takes place slightly more upstream (x=0.083 compared to 0.086) and a maximum temperature of 2600 K is reached at the duct exit. A combustion efficiency of 68% is reached. The flow in the spanwise symmetry plane is only affected by the combustion further downstream, where the temperature rises slightly.

The location of ignition and the shape of the combustion region resulting from the computations for HEG runs 667, 664 and 663 can be seen in Figures 9-11 where the H_2O concentration is plotted. The ignition takes place in the high temperature region behind the bow shock. However, since the mixing there is still low, full combustion is developed further downstream. With higher equivalence ratio, the penetration is increased and combustion takes place earlier. In addition, the separation in front of the injector is filled with hydrogen, which is ignited in the high temperature flow field at the bow shock.

Surface pressure plots of the lower combustion chamber wall are compared with the experimental data in Figures 12-14 for different equivalence ratios and flow conditions. Without combustion, represented by run 672 for which hydrogen was injected into nitrogen, the pressure increase due to the injected mass flow predicted by the numerical results is slightly lower than the experimental data (Figure 12). The pressure at the duct exit (x=0.3) reaches a dimensionless pressure (normalized with the free stream Pitot pressure) of 1.3; without injection it amounts to 1.2. Injecting hydrogen into air (run 667) or nitrogen (run 672) or a variation of the flow condition (663) does not cause a significant change of the surface pressure distribution.

The numerical calculation of the HyShot flight condition for the fuel off condition (Figure 13) shows that the pressure level of the flight experiment cannot be reached. However, good agreement with the experimental HEG data is obtained.

Pressure distributions including combustion are shown in Figure 14. The numerical result for run 667 shows a pressure rise of 25% to 1.63 compared with the no combustion case of Figure 12. Although the combustion takes place, the pressure increase is quite low. The experimental result shows a comparable pressure level, although the pressure increase and drop at x=0.2 cannot be reproduced numerically. The variation of the equivalence ratio according to the runs 664 and 663 show much smaller pressure increases than the experimental data. For run 664 (Φ=0.32) and 663 (Φ=0.35), the pressure increases slightly to 1.75 and 1.8; the experimental results on the contrary show maximum pressure levels of 2.3 (664) and 3 (663).

The discrepancies between flight experiment and HEG have been outlined and the sensitivities have been shown before[4,5]. According to these references, changes of the angle of attack have a large impact on the combustion process leading to major pressure level changes in the duct. The offset between numerical and experimental data may also be the result of using nominally the same but practically different hydrogen flow rates. The accuracy of the hydrogen mass flow is given with ±3%[4]. Run 663 was adapted to an equivalence ratio of 0.43 which leads to a maximum pressure value of 2.05 (Figure 14). The location of ignition and the shape of the combustion region for this case is shown in Figure 15.The flow is fully attached, whereas the combustion is enhanced compared to Figure 11.

Increasing the equivalence ratio further to 0.55 (Figures 16 and 17) and 0.71 (Figures 18 and 19) enhances the combustion significantly. The flow topology indicates a separation zone behind the injector in the injector symmetry plane. Due to this, the recirculation acts as a flame holder increasing combustion and hence also the pressure. The separation in front of the injector is increased and filled with hydrogen which is immediately ignited. Inside the combustion chamber, the pressure is increased to a dimensionless value between 3.05 (Φ=0.71) and 3.2 (Φ=0.55).

At the combustion chamber symmetry plane downstream the separation the flow is slightly subsonic. The Korkegi formulation, which is an empirical prediction for flow separation of the boundary layer due to an adverse pressure gradient, predicts maximum dimensionless pressure values between 2.39 (663) and 2.47 (672) before separation would occur:

$$\frac{p}{p_i} = 1 + 0.3 \cdot Ma^2, \quad \text{Ma} \leq 4.5.$$

V. Summary

In the present study, numerical computations were performed related to experimental investigations of the HyShot configuration at a Mach number of 7.8 and a corresponding altitude of 27 km in HEG. In summary it can be stated that the pressure distribution inside the combustion chamber can be adjusted in both the CFD and the experiments, by varying the angle of attack and/or the fuel equivalence ratio. Concerning the latter, experimental investigations will be performed in the near future to measure this quantity with higher accuracy. Analyzing the present data leads to the conclusion, that in run 667 and 664 in HEG the combustion takes place in an attached supersonic flow with a continuous increase in pressure along the duct, whereas in run 663 and in the HyShot flight experiment a local separation in the combustion chamber behind the injector might have occurred, enhancing the combustion heat release significantly in partially subsonic flow, whereas the overall duct flow stays supersonic. A further difference between flight and HEG is the wall surface temperature, which is higher during flight. This would reduce the ignition delay in the wall near regions. Investigations using CFD will be performed in the future to study this.

Although the main physical effects seem to be well captured, the present results should be regarded as a first step, since the interaction of the turbulent flow and the combustion process was not modeled. Further, the influence of using different turbulence models on the mixing process needs to be investigated. This will be done in further investigations in the near future.

Acknowledgments

The numerical work was performed within the 'Long-Term Advanced Propulsion Concepts and Technologies' project investigating high-speed airbreathing propulsion. LAPCAT, coordinated by ESA-ESTEC, is supported by the EU within the 6th Framework Programme Priority 1.4, Aeronautic and Space, Contract no.: AST4-CT-2005-012282. Further info on LAPCAT can be found on http://www.estec.esa.int/techresources/lapcat.

References

[1]Paull, A.,Scramjet measurements in a shock tunnel. AIAA 99-2450, 1999

[2]Beck, W.H., Hannemann, K., Weiland, M., Modifications to the DLR high enthalpy shock tunnel HEG for measurements on supersonic combustion. AIAA 2001-1860, 2001

[3]Paull, A., Alesi, H., Anderson, S., HyShot flight program and how it was developed, AIAA 2002-4939, 2002

[4]Gardner, A.D., Hannemann, K., Evaluation of Full Engine Scramjet technology. DLR-IB 224-2004 A 11, 2004

[5]Gardner, A.D., Hannemann, K., Steelant, J., Paull, A. Ground Testing of the HyShot Supersonic Combustion Flight Experiment in HEG and Comparison with Flight Data, AIAA 2004-3345, 2004

[6]Mack, A., Hannemann, V., Validation of the Unstructured DLR-TAU-Code for Hypersonic Flows, AIAA 2002-3111

[7]Adeli, R., Flow Filed Study due to a Supersonic Jet Exiting into a Supersonic Stream. Proceedings of 14th STAB Symposium, Bremen, Germany, November 16-18, 2004

[8]Kovar, A., Schülein, E., Comparison of Experimental and Numerical Investigations on the Side Jets in a supersonic Cross Flow. Royal Aeronautical Society, London, Great Britain, September 14-15, 2004

[9]Karl, S., Hannemann, K., Application of the DLR Tau-code to the RCM-1 testcase: Penn State Preburner Combustor. Proceedings of the 3rd International Workshop on Rocket Combustion Modeling, 2006

[10]Evans, J.S., Schexnayder Jr., C.J., Influence of Chemical Kinetics and Unmixedness on Burning in Supersonic Hydrogen Flames AIAA Journal, Vol. 18, No. 2, February 1980

Annex

	HEG 663	HEG 664	HEG 667	HEG 672	HyShot flight
Ma_∞ [-]	7.8	7.8	7.8	7.8	7.74
T_∞ [K]	242.0	234.6	231.8	235.5	219.7
p_∞ [N/mm^2]	1710.8	1625.4	1680	1705.6	1780.0
α [^{o}]	3.64	3.62	3.58	3.61	3.6
$\dot{m}$ (H_2) [g/s]	3.78	3.34	2.75	3.32	3.78
Φ [-]	0.345	0.317	0.251	0.297	0.320

Table 1: Free stream and fuel injection conditions used in HEG experiments

Figures

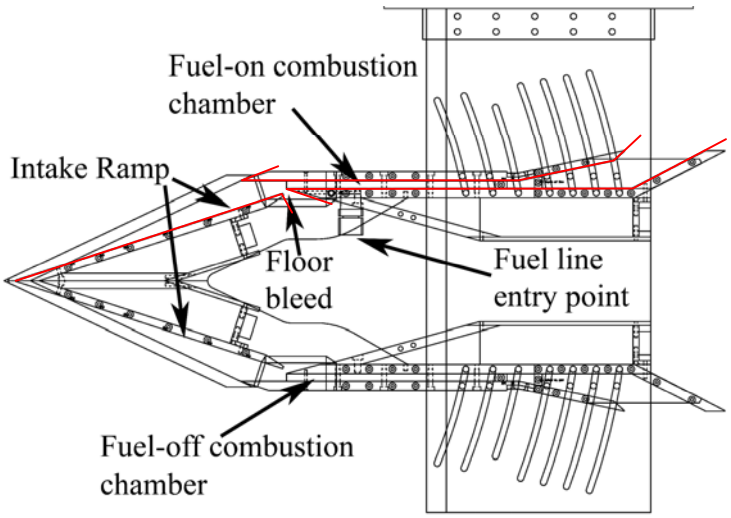

Figure 1: HEG generic wind tunnel model (Gardner and Hannemann[4])

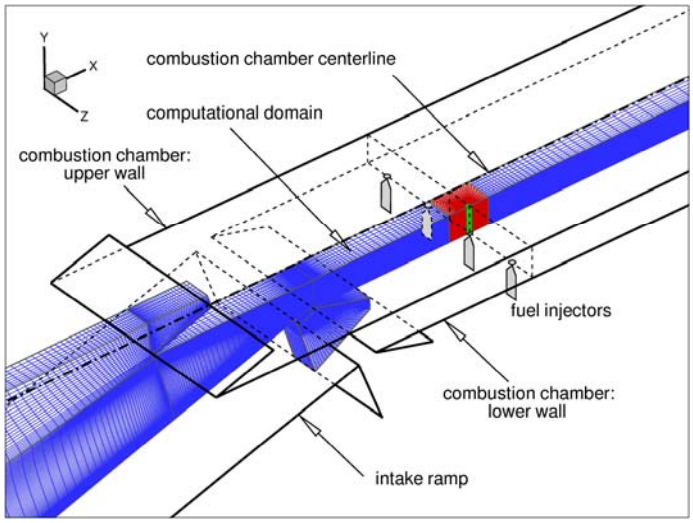

Figure 2: Fuel injection and computational domain

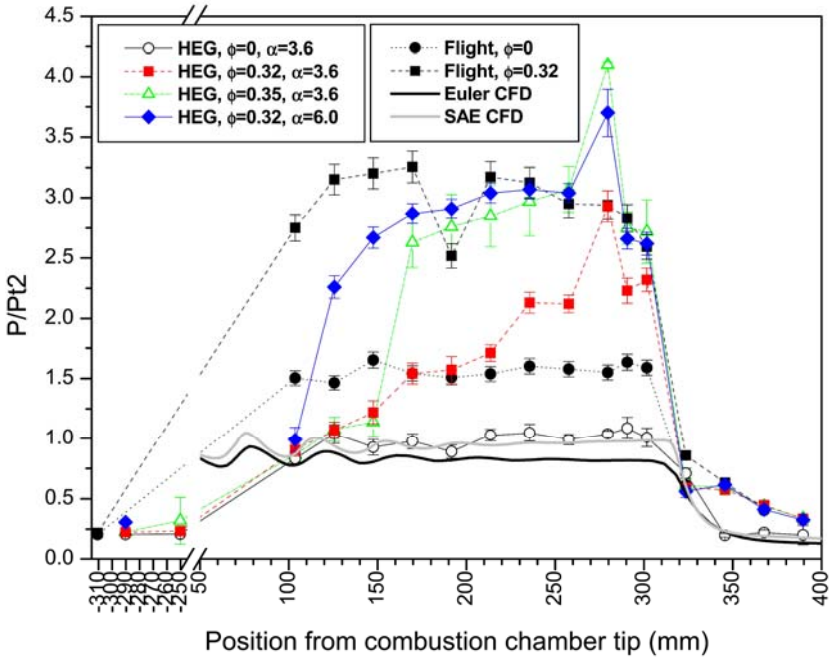

Figure 3: Comparison of wall pressures between experimental, flight and fuel-off CFD data (Gardner et al.[5])

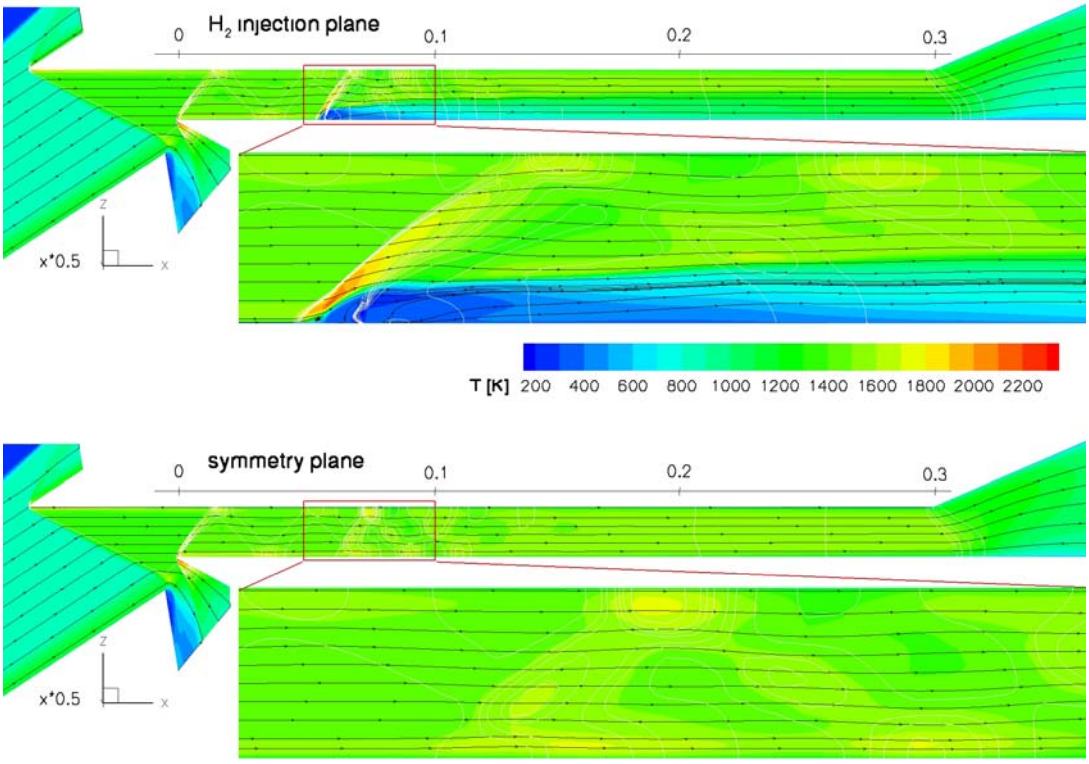

Figure 4: Run 667 (no combustion), flow topology including streamlines, pressure isolines and temperature

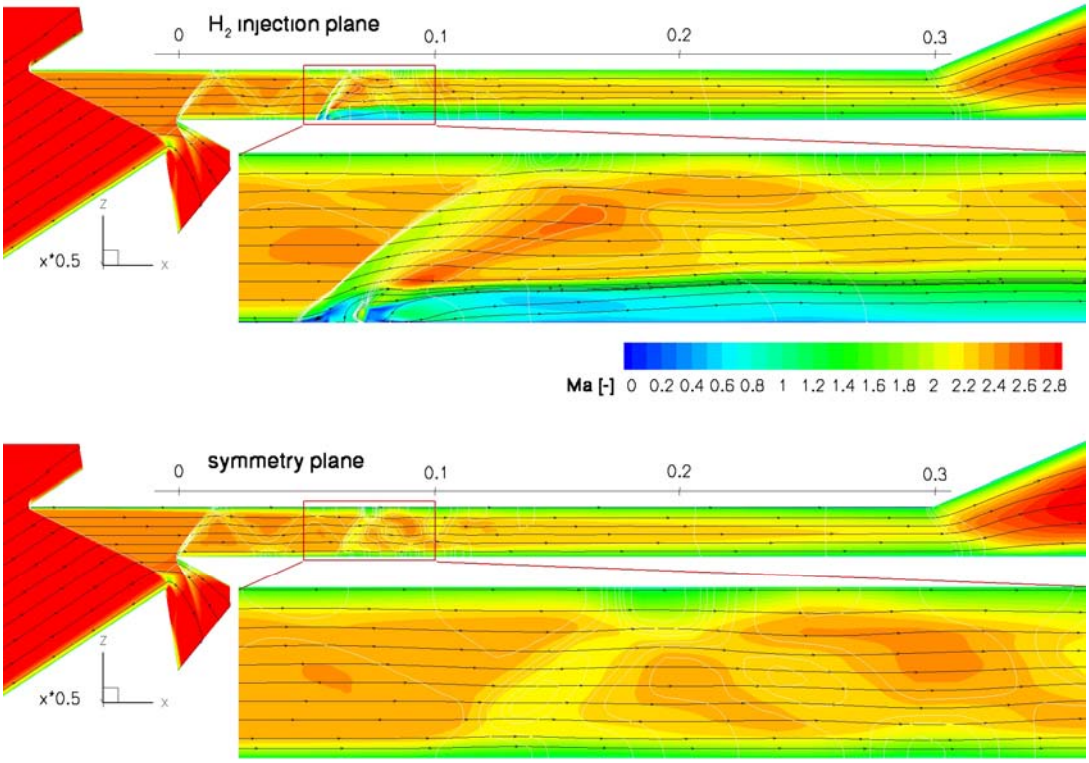

Figure 5: Run 667 (no combustion), flow topology including streamlines, pressure isolines and Mach number

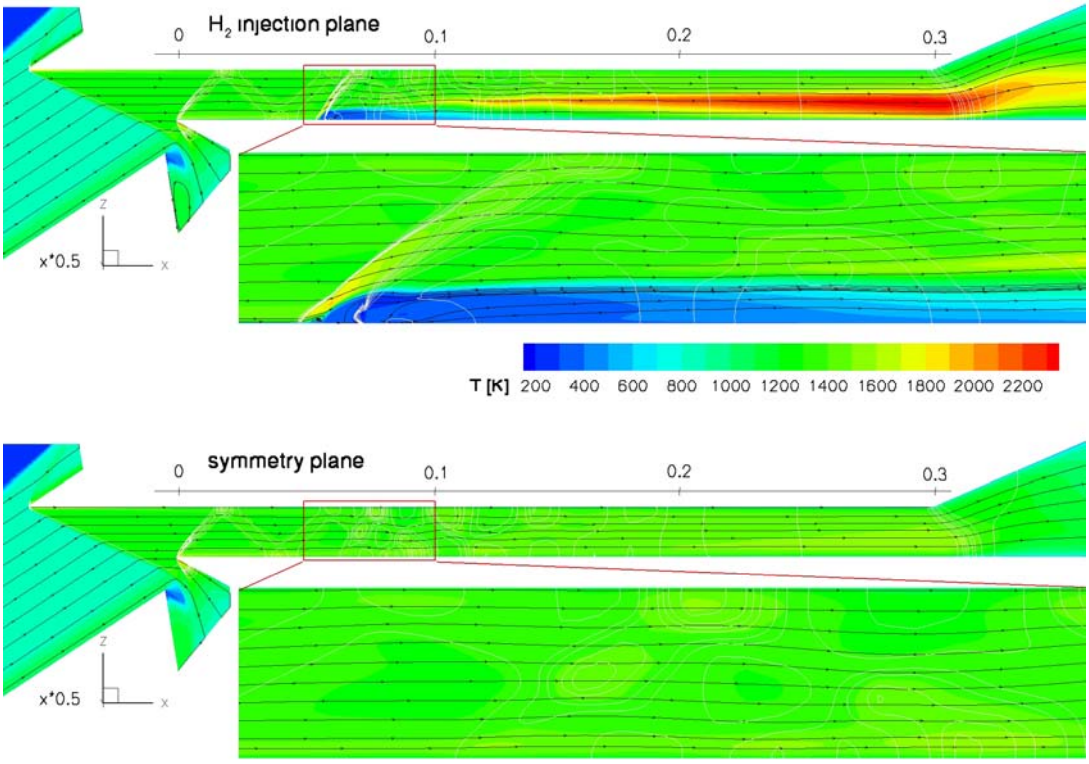

Figure 6: Run 667 (with combustion), flow topology including streamlines, pressure isolines and temperature

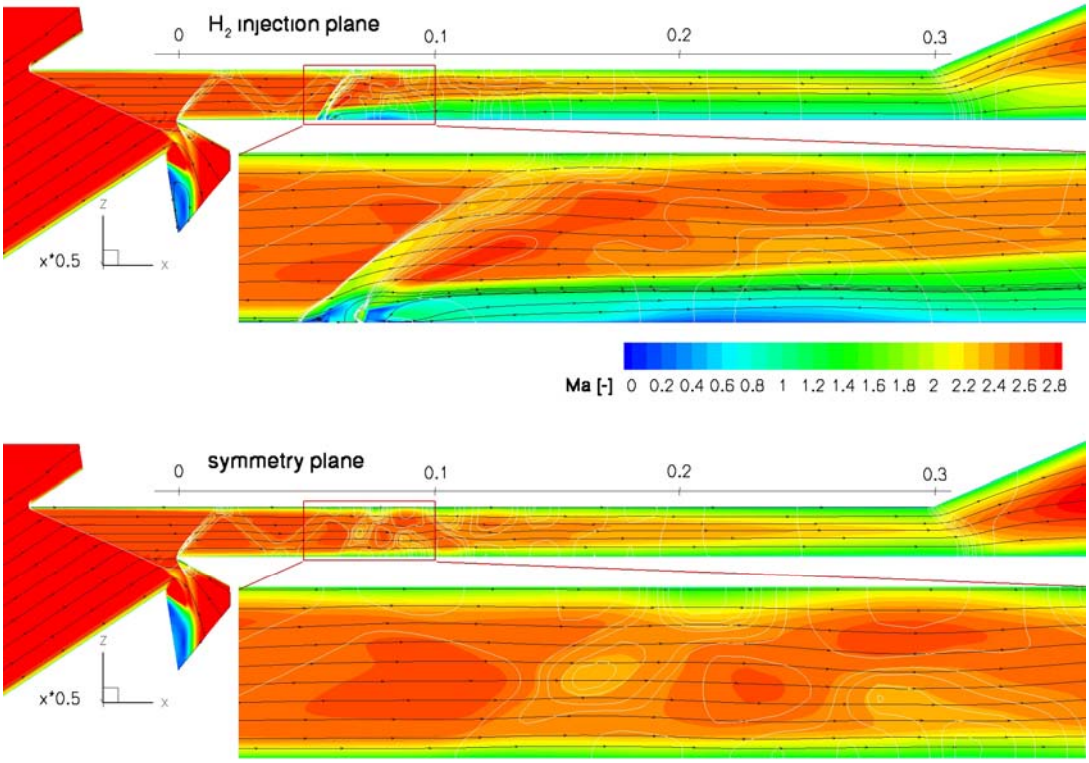

Figure 7: Run 667 (with combustion), flow topology including streamlines, pressure isolines and Mach number

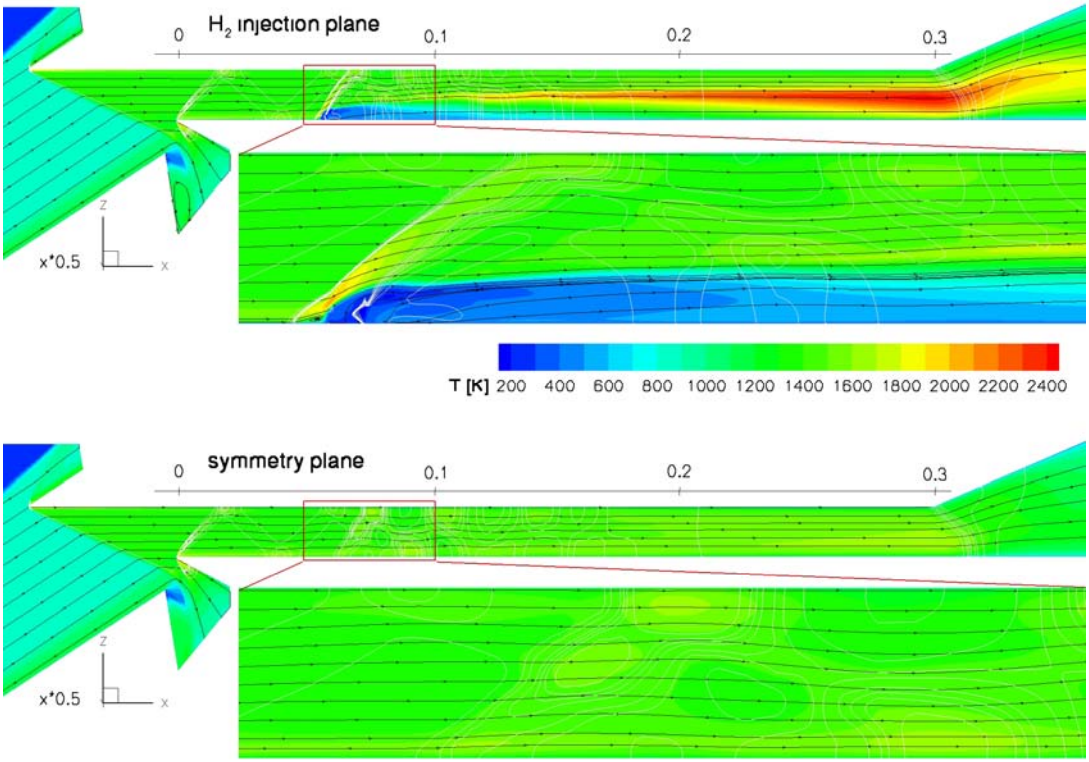

Figure 8: Run 663 (with combustion), flow topology including streamlines, pressure isolines and temperature

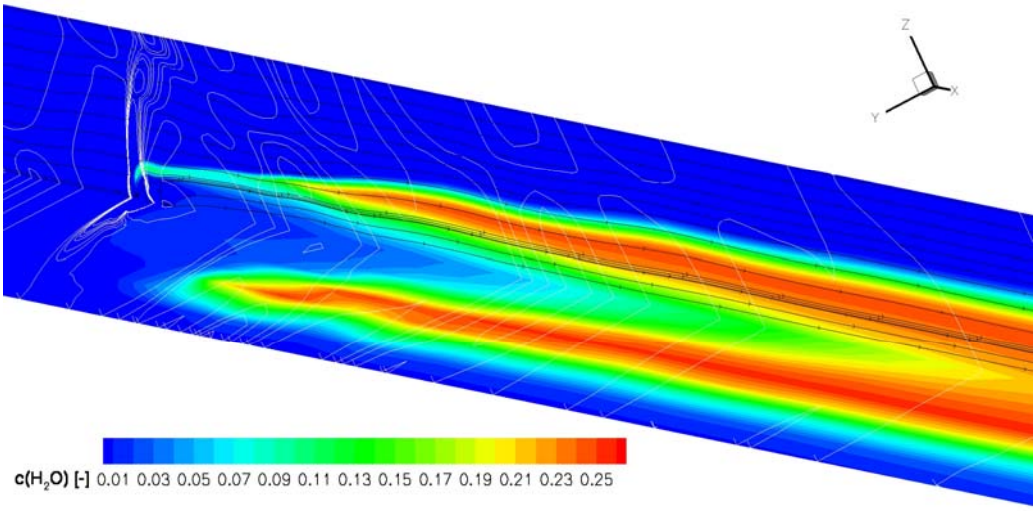

Figure 9: Run 667, H_2O concentration, pressure isolines and flow field topology in the vicinity of the Injector (x=0.033 to 0.2)

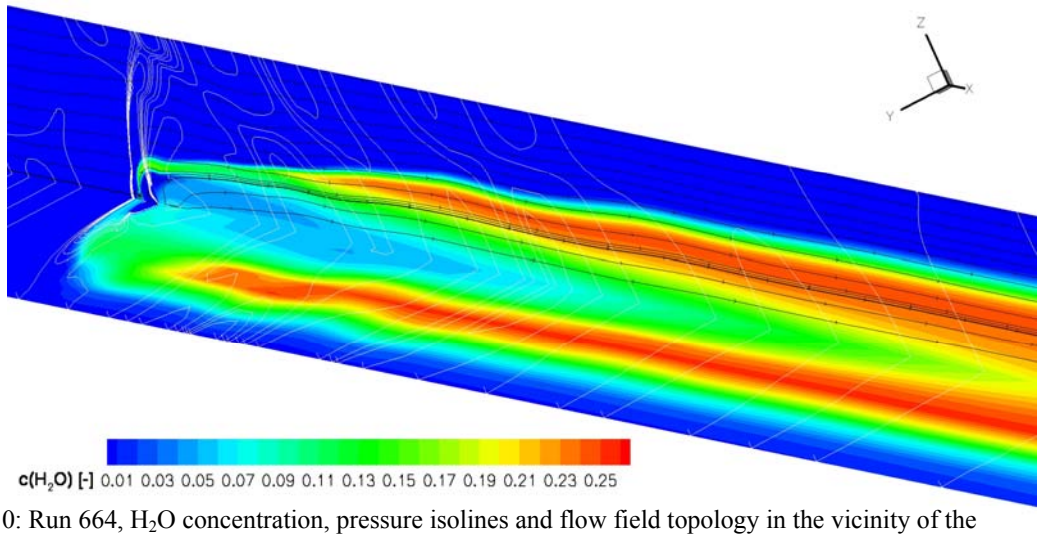

Figure 10: Run 664, H_2O concentration, pressure isolines and flow field topology in the vicinity of the injector (x=0.033 to 0.2)

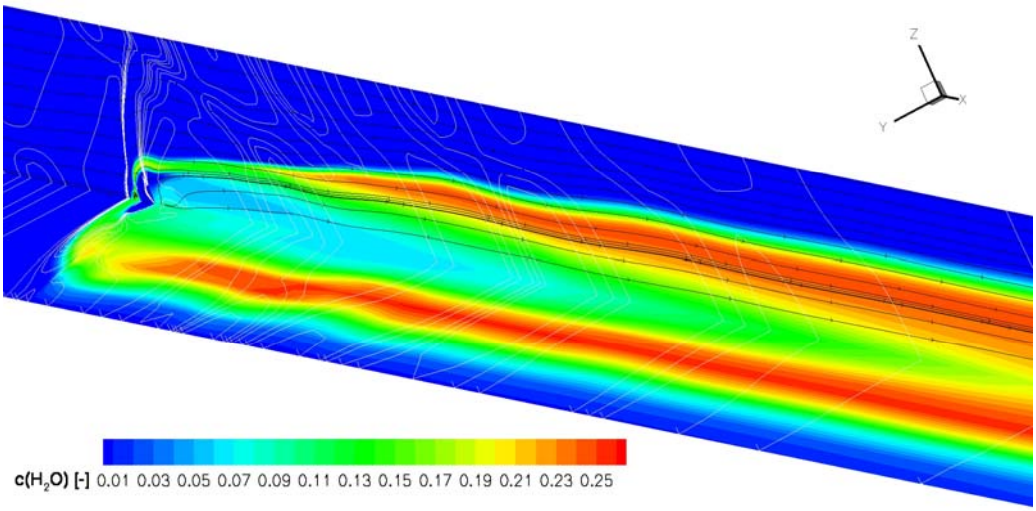

Figure 11: Run 663, H_2O concentration, pressure isolines and flow field topology in the vicinity of the injector (x=0.033 to 0.2)

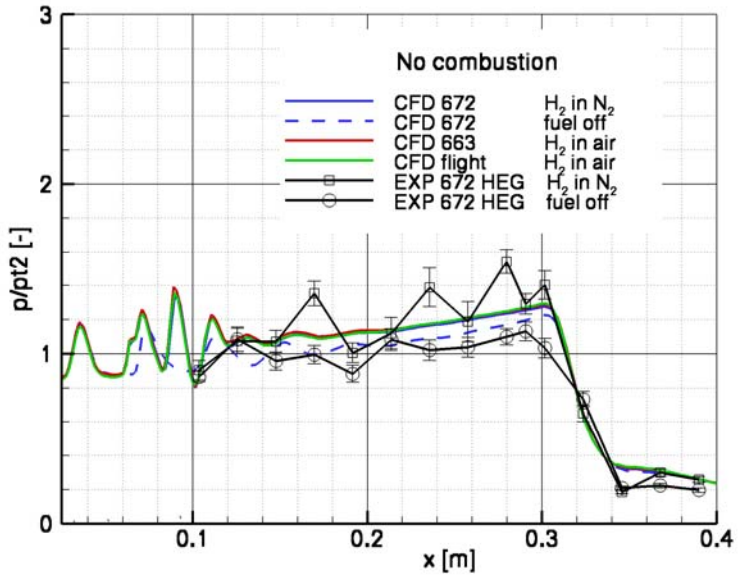

Figure 12: Comparison of surface pressures resulting from CFD solutions and experiments (HEG, HyShot flight) for flows without combustion

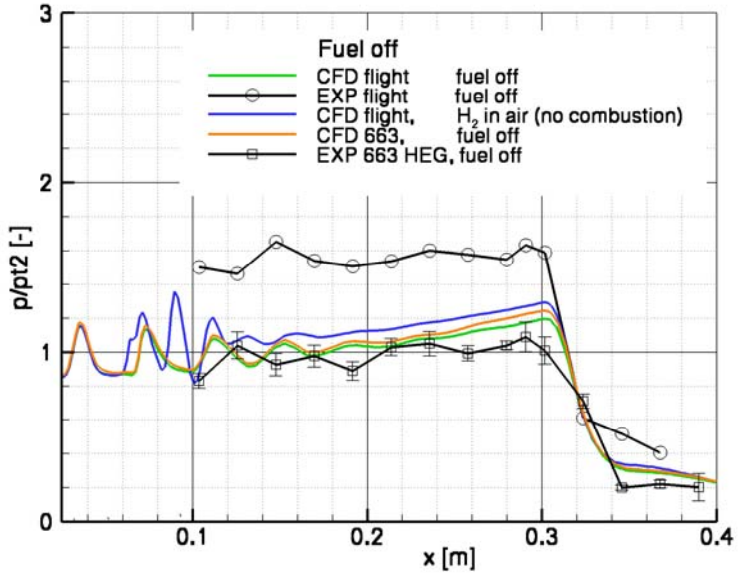

Figure 13: Comparison of surface pressures resulting from CFD solutions and experiments (HEG, HyShot flight) for fuel off/no combustion flows

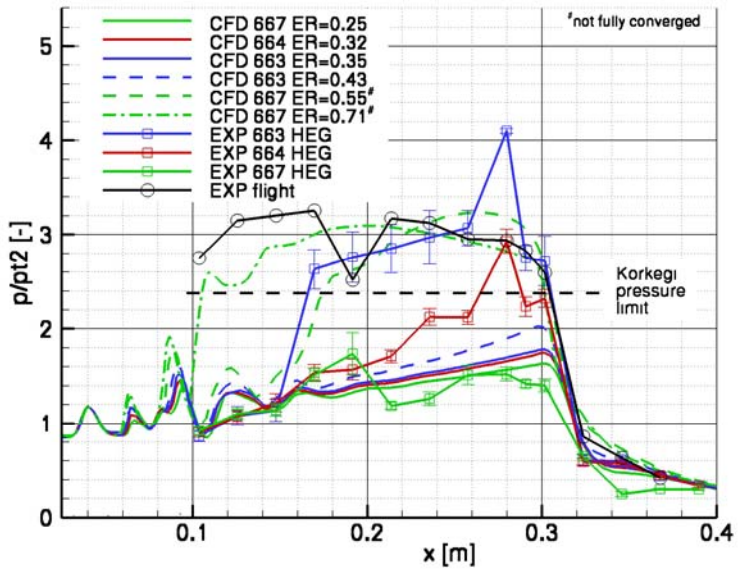

Figure 14: Comparison of surface pressures resulting from CFD solutions and experiments (HEG, HyShot flight)

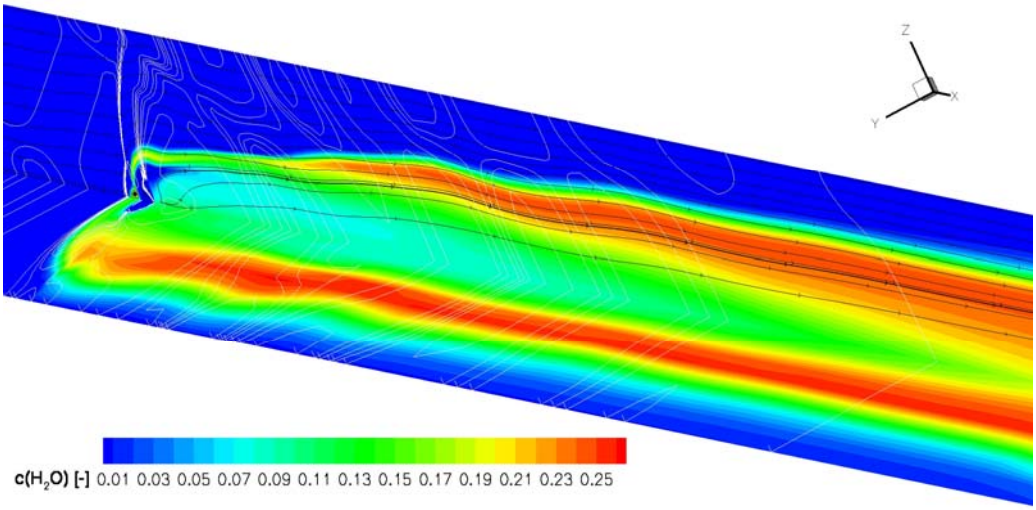

Figure 15: Run 663 (Φ=0.43), H_2O concentration, pressure isolines and flow field topology in the vicinity of the injector (x=0.033 to 0.2)

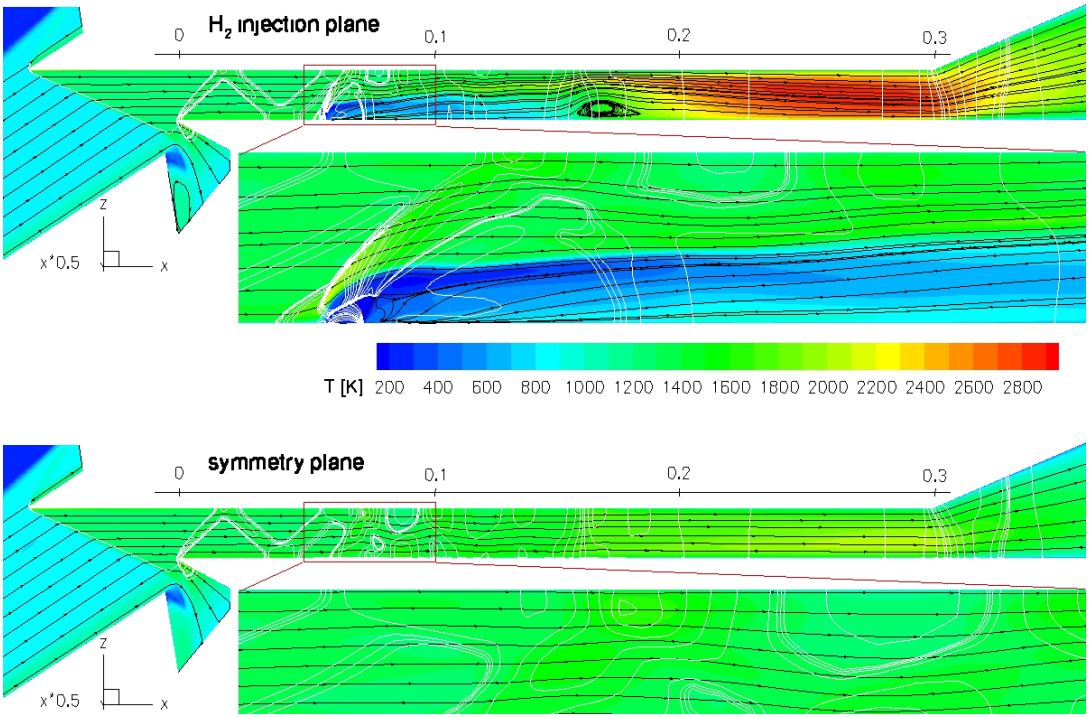

Figure 16: Equivalence ratio sensitivity analysis run 667 (Φ=0.55), flow topology including streamlines, pressure isolines and temperature

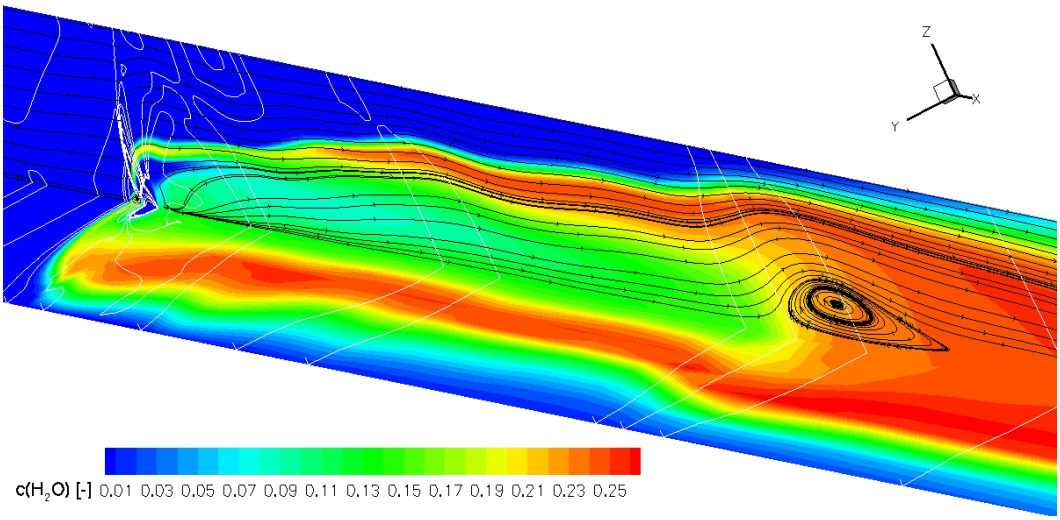

Figure 17: Equivalence ratio sensitivity analysis run 667 (Φ=0.55), H_2O concentration, pressure isolines and flow field topology in the vicinity of the injector (x=0.033 to 0.2)

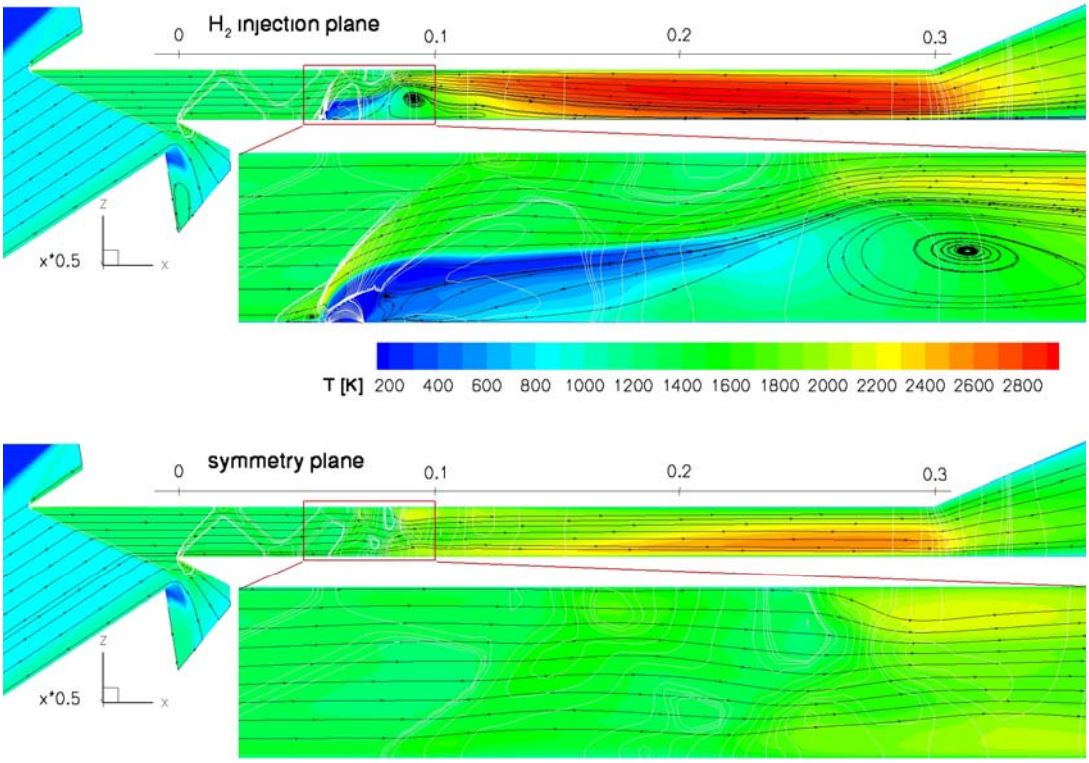

Figure 18: Equivalence ratio sensitivity analysis run 667 (Φ=0.71), flow topology including streamlines, pressure isolines and temperature

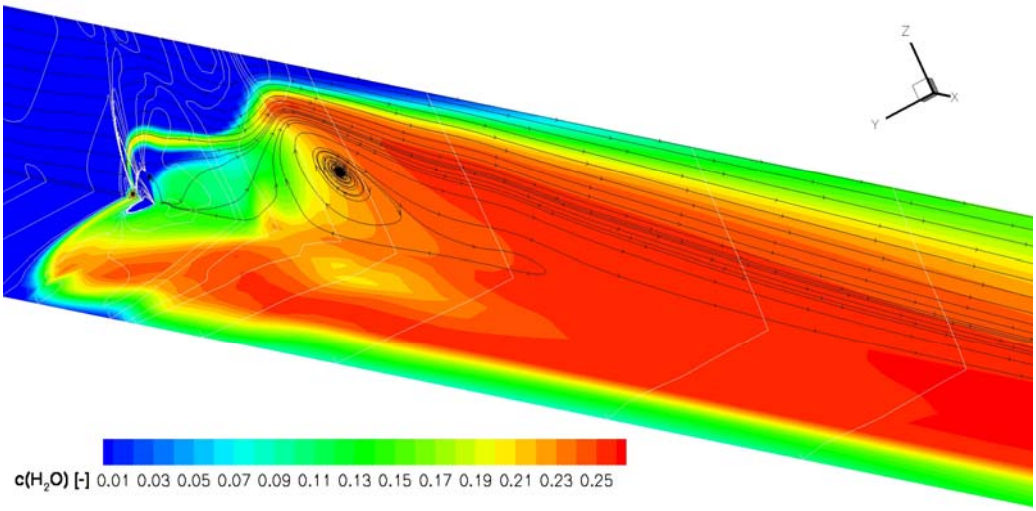

Figure 19: Equivalence ratio sensitivity analysis run 667 (Φ=0.71), H_2O concentration, pressure isolines and flow field topology in the vicinity of the injector (x=0.033 to 0.2)